Mineralization of titania with sfGFP-Car9 variants

ChiaWei Hsu

A thesis
submitted in partial fulfillment of the
requirements for the degree of

Master of Science in Chemical Engineering

University of Washington
2017

Committee:

François Baneyx

Cole DeForest

Program Authorized to Offer Degree:

Chemical Engineering

University of Washington

Abstract

Mineralization of titania with sfGFP-Car9 variants

ChiaWei Hsu

Chair of the Supervisory Committee:

François Baneyx, Chairman

Department of Chemical Engineering

Biomineralization is a process that emulates nature's way of producing nanostructured materials under benign conditions and with the aid of biomolecules. It offers an environmentally friendly alternative for synthesizing inorganic compared to traditional processing and fabrication routes that involve energy-intensive and high temperature processes. In this work, we investigate how variants of superfolder green fluorescent protein (sfGFP) incorporating a panel of solid binding peptides (SBPs) modulate the precipitation of titania (TiO_2) under non-equilibrium conditions using a new coffee ring effect (CRE) biomineralization approach. By depositing a small droplet containing various engineered solid-binding peptides on an agarose substrate supplemented with the soluble titanium

precursor, titanium(IV) bis(ammonium lactato) dihydroxide (TiBALDH). We show that diffusion-reaction leads to the formation of distinct patterns of precipitated TiO_2. Using image analysis and SEM, we take the first steps towards correlating the macroscopic and microscopic characteristics of the dynamically formed precipitate with protein concentration, solution viscosity, the amino acid composition, insertion point and valency of the SBPs incorporated within the sfGFP framework.

Acknowledgement

I would like to acknowledge those who have helped me in the development of my master study and thesis. First, I would like to thank my principal investigator, Dr. François Baneyx for his instruction and mentorship throughout these two years, offering me the opportunity to dig into the charming molecular biology field.

I would also like to acknowledge my colleagues in Baneyx's lab: Dr. Brian Swift, Jessica Soto-Rodriguez, for always kindly answering my questions; Alexander Thomas, for bringing the laughter to the lab; Brittney Hellner, for your continuous assistant during my project; Sonja Dunakey, for being my classmate and teaching me a lot when I enter the Baneyx's lab; Wenlan Yang and Kannan Aravagiri, for sharing and leading my master study; Meng Xu, Tong Zhang and YaTong Ge, for your Chinese version of teaching that makes me learn a lot.

Finally, thank you to my family, for your support throughout my entire master study. You were always there to encourage me and gave me the strength to move on.

Introduction

Traditional synthesis of inorganic materials requires harsh conditions, such as thermal decomposition, extremes of pH and caustic environments.[1,2,6,7] Biomineralization, on the other hand, is a natural precipitation or reduction process that is driven by biomolecules, and results in the synthesis of compositionally and structurally complex inorganic materials under environmentally benign conditions.[1-8]

Titania (TiO_2) nanoparticles are very attractive materials that are frequently used in photocatalysis, in energy storage, pigments and sunscreen applications.[1,5,9] The technological performance of titania is highly dependent on physical properties, such as particle size and crystallinity.[5] Biomolecules, especially proteins and peptides, have shown promise in controlling of the morphology of mineralized titania.[6,7] Here, we take advantage of the ability of solid binding peptides (SBPs) to modulate the nucleation and growth of inorganic materials at low concentration when incorporated within larger protein scaffolds to study titania biomineralization under non-equilibrium conditions.[7,10,12-14] Solid binding peptides are short amino acid sequence that bind to specific materials through multiple non-covalent interactions, such as electrostatic, hydrophobic and hydrogen bonds.[13,14] More specifically, we use a panel of such designer proteins constructed by fusing wild type and mutant versions of Car9 (Table 1), a dodecapeptide that binds to sp^3-hybridized carbon substrates as well as

silica[11,28] to the C-terminus of superfolder green fluorescent protein (sfGFP) through a flexible linker.[11] By exploiting the ability of the Car9 tag to bind to silica, these fusion proteins can be affinity purified on silica gel columns rapidly and inexpensively.[11]

Table 1
Car9 tag mutation with its specific objectives

	Sequence	Objectives
Wild type	DSARGFKKPGKR	-
F6A	DSARGAKKPGKR	Hydrophobic core
K8HK11H	DSARGHKHPGHR	Effects of pH
R4QR12Q	DSAQGFKKPGKQ	Role of R4 and R12
K8AK11A	DSARGFKAPGAR	Role of K8 and K11
K7AR12A	DSARGFAKPGKA	Role of K7 and R12
P9AG10A	DSARGFKKAAKR	Effect of hairpin

The choice of sfGFP as a protein scaffold is motivated by its improved thermo-stability and the presence of a permissive site within loop 9 that tolerates the insertion of extraneous amino acids up to 20 residues in length.[28] An SBP inserted at this position lies opposite to the protein's N- and C-termini (Figure 1).

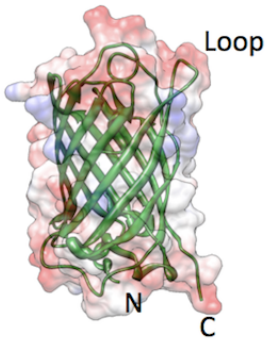

Figure 1. Loop, N-, C-termini labeled sfGFP

Variants of sfGFP containing an N-terminal Car9 extension(Car9-sfGFP), a C-terminal Car9 extension (sfGFP-Car9), a loop 9 insertion (sfGFP::Car9), as well as dual-tagged Car9 variants have been constructed and purified by the Baneyx's lab.

The coffee ring effect (CRE) describes a phenomenon that occurs when evaporation of a colloidal droplet on a solid surface leaves behind a dense deposit at the edge.

CRE is named after the ring of coffee particles that appear upon evaporation of coffee drops and is important in applications that range from inkjet printing,[30,31] to protein microarrays,[32] and chromatography.[33] CRE was first investigated and explained by Deegan and coworkers.[15-17] In our system, a droplet of colloidal protein suspension is deposited on an agarose hydrogel containing the titanium precursor, TiBALDH in an acidic citrate buffer. Protein molecules pinned at the liquid-gas-solid contact line precipitate the precursor to form titania (TiO_2). At the same time, solvent evaporation near the contact line generates a capillary flow towards the droplet edges to replenish the lost fluid. [17-20] This flow also brings about a progressive increase in the concentration of the protein solute at the droplet periphery, which drives additional TiO_2 precipitation.

In this work, we evaluate how a number of experimental variables including pH, viscosity, protein framework, amino acid composition, and position and number of Car9 motifs influence titania precipitation outcomes.

Materials and Methods

I. Protein expression

Seed cultures (25ml) of BL21(DE3) cells harboring pET24(+)-sfGFP, pET24(+)-sfGFP-Car9, and pET24(+)-mCherry-Car9 were used to inoculate 500 mL of LB medium supplemented with 50 μg/ml of kanamycin. Cells were grown to A_{600}=0.5 at 37 °C and cultures were treated with 500 μL, 1M isopropyl β-D-thiogalactopyranoside (IPTG) to induce recombinant protein synthesis. After 5 hours of incubation at the same temperature, cells were harvested by centrifugation at 7000*g* for 10 min. Pellets were resuspended in 35 mL of 20 mM Tris-HCl, pH 7.5 (Buffer A) supplemented with 2 mM EDTA and 1 mM PMSF, and disrupted by six cycles of sonication on a Branson sonifier for 3 min at 30% duty cycle. The lysates were clarified by centrifugation at 10000*g* for 15 min. Supernatants were heat shocked at 50 °C (mCherry-Car9) or 70 °C (sfGFP and sfGFP-Car9) for 10 min to promote the aggregation of thermolabile proteins. Insoluble material was removed by centrifugation at 10000*g* for 15 min.

II. Protein purification

For Car9-tagged proteins, 6g of silica gel (35-60 mesh, 15 nm pore size, Sigma-Aldrich) was washed with Buffer A three times, and the slurry was incubated with cell lysates prepared as described as above on a Dynabeads sample mixer (Invitrogen) at 60 rpm for 10 min. The material was then packed in a 1 cm inner diameter chromatography column (GE Healthcare)

that was washed with Buffer A until no protein was detected in the effluent. Proteins were eluted using Buffer A supplemented with 1M L-lysine as reported.[11,12] Untagged sfGFP was purified by fast protein liquid chromatography (FPLC) on a Whatman DE52 anion exchange cellulose column (GE Healthcare). Purified proteins were dialyzed against 3 L of buffer A using 10-kDa MWCO SnakeSkin tubing (Thermo Scientific) and subjected to 3 buffer change to remove lysine. Proteins were concentrated with 10-kDa microconcentrators (Merck). Protein concentrations were determined by BCA Protein Assay Kit (Thermo Scientific). Protein purity was determined by SDS-PAGE analysis. Proteins were then aliquoted and stored at -20 °C.

III. Car9 mutant proteins construction and expression

Car9 mutant proteins were constructed by Brittney Hellner (Baneyx lab) using pET-24(+)-sfGFP-Car9 as a starting point. Briefly, pET-24(+)-sfGFP-Car9 was digested with *Hind*III and *Xho*I to remove the DNA segment encoding wild type Car9 and oligonucleotides containing the desired mutations were annealed, digested with the same enzymes and cloned within the linearized backbone. Mutant plasmids were transformed into BL21(DE3) cells and protein expression and purification were performed as with wild type sfGFP-Car9.

IV. Titania mineralization on thin agarose film

Ultrapure™ agarose (Invitrogen) was used for all experiment. TiBALDH was purchased from Sigma Aldrich. Agarose powder (0.40g) was added to 20 mL ddH_2O water to form a 2% (wt/vol) agarose solution in a 50-mL beaker and the powder was dissolved using 4 cycles of 20 second heating in a microwave. Meanwhile, 88 µL of stock (1.7M) TiBLADH was mixed with 2912 µL of citrate buffers prepared as described,[29] and the solution was transferred to a 70°C water bath for 30 min. The solution (3 mL) was mixed with 3 mL of 2% agarose. Final concentration was 25 mM TiBALDH, 1% agarose and citrate buffer at specified pH. The mixture was poured in a 90-mm diameter petri dish to form a thickness of 1 mm thick film that was allowed to gel at room temperature for 1 hour with the petri dish lid on. Next, 5 µL of protein solution was transferred to a PCR tube from which a 0.5 µL protein droplet was withdrawn and slowly deposited on the TiBALDH-containing agarose without touching the surface by a 0.1-10 µL P2/P10 Ultra Micro Pipet Tips (Fisherbrand). Protein solutions in the PCR tubes were disposed of after one use.

V. Deposition Pattern Analysis

Deposition patterns were imaged by phase contrast under 4X and 20X magnification on a Nikon Eclipse TE2000-U fluorescent microscope 2 hours after protein droplets deposition. Fluorescent microscopy images were acquired under blue light (sfGFP) and green light

(mCherry) excitation. Image analysis was carried out using the NIH ImageJ software. Intensity analysis for single droplet was carried out by averaging the intensity profiles from three lines scans crossing the center of the droplet and collecting at 0° (arbitrary), +120° and -120° angle using the "Plot Profile" tool in ImageJ. Each experiment was repeated a minimum of three times.

VI. SEM Imaging of TiO_2 Precipitates

Titania mineralized by depositing forty 0.5 µL droplet of a 50 µM of sfGFP-Car9 and F6A mutation was recovered by excising the underlying agarose with a razor blade. Samples were transferred to a 1.7 ml Eppendorf tube. The agarose was dissolved in 1mL of bleach (6% Sodium hypochlorite) with heating at 70 °C for 30 min. Mineralized titania was recovered by centrifugation at 10000*g* for 10 min. The titania pellet was washed three time with ddH_2O and resuspended in 100 µL of ddH_2O. An aliquot (3 µL) was deposited on a silicon wafer, air-dried overnight, and imaged on a FEI Sirion XL30 SEM at various magnifications.

Results and Discussion

We first used wild type sfGFP and sfGFP-Car9 to explore the biomineralization of titania on thin (1 mm) agarose substrates containing 25 mM of the titanium precursor TiBALDH in citrate buffers held at different pH values. The mechanism of titania biomineralization is not fully understood. We speculate that the bidentate lactate ligands of TiBALDH are destabilized under acidic conditions and that positively charged amino-acids (Lysine, Arginine and Histidine) in peptides and proteins are believed to concentrate the negatively charged titanium oxide clusters through a combination of electrostatic interactions and hydrogen bonding, promoting the formation of either edge-sharing or corner-sharing Ti-O-Ti bonds. Different stacking ways of TiO_6 octahedra will produce different crystal structures although biomineralized titania is usually amorphous (Figure 2).[2,4,5,34,35]

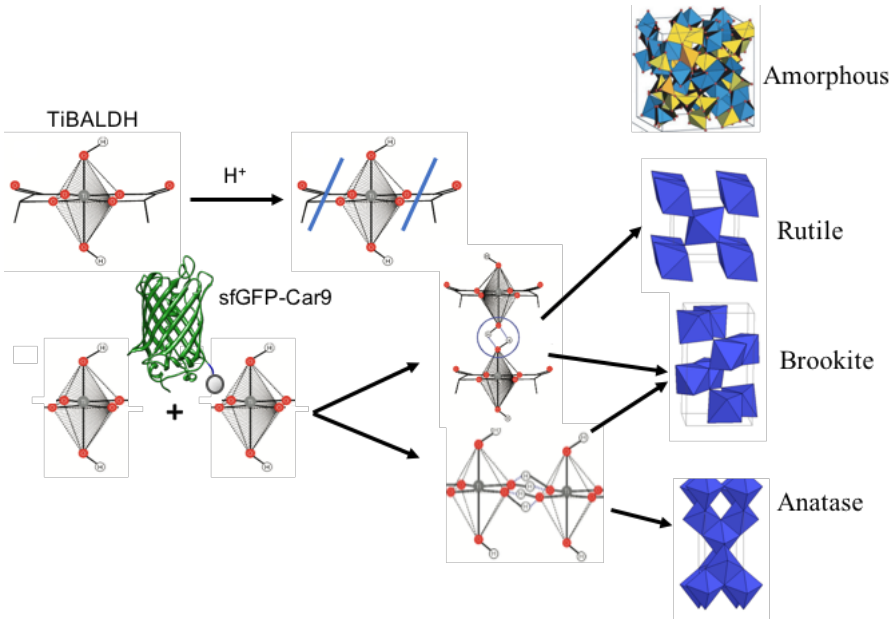

Figure 2. Putative scheme for sfGFP-Car9-induced TiO_2 mineralization under acidic conditions from precursor TiBALDH.

Influence of pH

Previously, we demonstrated protein-aided precipitation of TiO_2 by adding 5 µM of wild type sfGFP or sfGFP-Car9 to a solution of 25 mM TiBALDH prepared in citrate buffer solutions held at well-defined pHs (Figure 3). These experiments have revealed that acidic conditions are essential for precipitate formation since no titania is formed above pH 5.4, and that the Car9 extension does not improve the process when the pH decreases below 4.6. We therefore hypothesized that a pH of 5.0 would be ideal to delineate the contribution of the Car9 tag on titania mineralization.

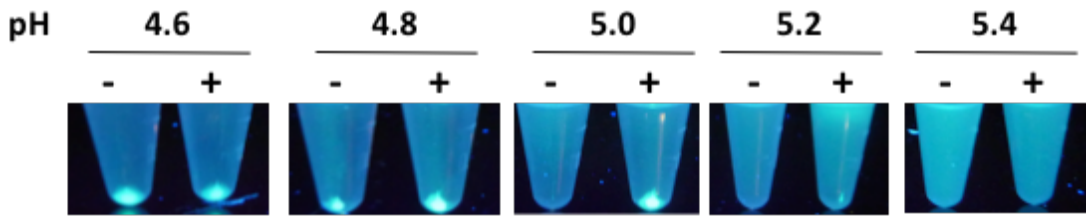

Figure 3. Mineralization of titania by addition of 5 µM sfGFP (-) or sfGFP-Car9 (+) to a solution of citrate buffer prepared at the indicated pH and containing 25 mM TiBALDH. The tubes were centrifuged and photographed under UV illumination to show the precipitated TiO_2 (Figure courtesy of Brittney Hellner, Baneyx's lab).

CRE mineralization experiments confirmed that both sfGFP and sfGFP-Car9 are efficient precipitators of titania at pH 4.8. This means that the Car9 extension contributes little to the materilzation process under acidic conditions (Figure 4 a, d). As expected from the result of Figure 3, the contribution of the Car9 extension becomes more important at pH 5.0 (Figure 4 b, e), suggesting that additional and/or co-located lysine and arginine residues are required to

destabilize the precursor and drive condensation reaction. Also, consistent with solution phase experiment, neither sfGFP nor sfGFP-Car9 were capable of inducing TiO_2 mineralization at pH 5.2 (Figure 4 c, f). Precipitation outcomes are even more obvious in the fluorescent images of Figure 5. At pH 4.8, both proteins precipitate titania, but there is some difference. Titania mineralized by sfGFP is mainly confined to the edges while the material mineralized by sfGFP-Car9 is more uniformly distributed. At pH 5.0, only sfGFP-Car9 induces mineralization with abundant precipitations at the edges and more sporadic precipitation events as one moves toward the center. We conclude that the Car9 extension can have a significant effect on the efficiency of titania precipitation but that is only does so within a narrow range of pH.

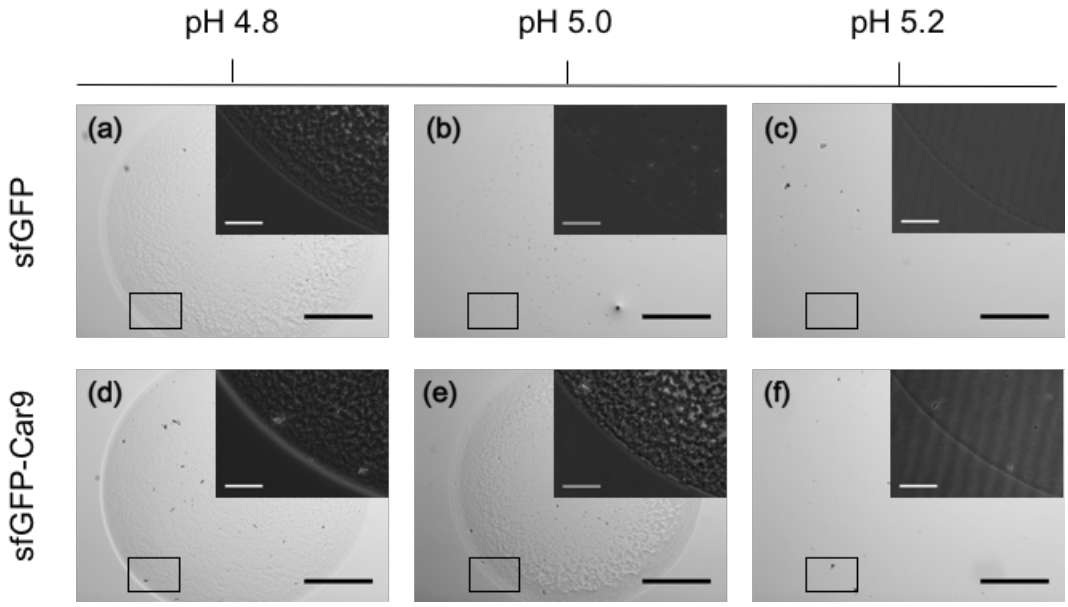

Figure 4. Bright field 4X (large) and 20X (insets) images of titania precipitated by a 0.5 µL droplet of 25 µM sfGFP or sfGFP-Car9. The 1% agarose substrates contained 25 mM TiBALDH and were maintained at pH 4.8, 5.0, 5.2 using citrate buffers. Scale bars correspond to 500 µm for 4X images and 100 µm for the insets.

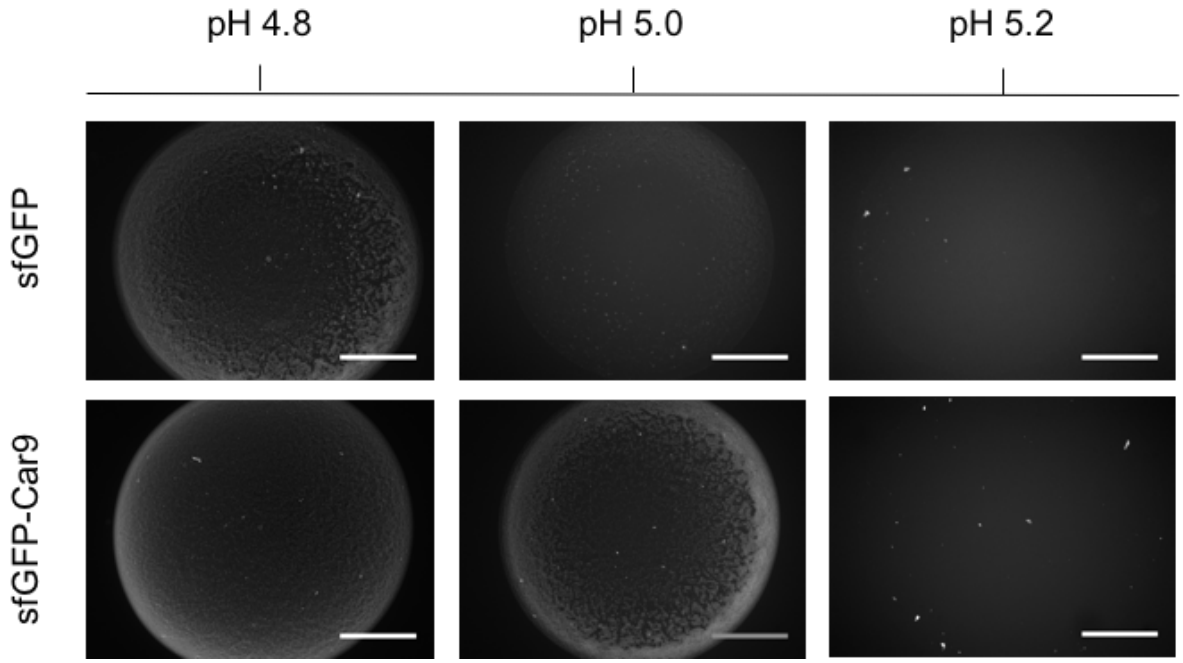

Figure 5. Fluorescent images (4X magnification) of titania precipitated by a 0.5 µL droplet of 25 µM sfGFP or sfGFP-Car9. The 1% agarose substrates contained 25 mM TiBALDH and were maintained at pH 4.8, 5.0, 5.2 using citrate buffer. Scale bars correspond to 500 µm.

Influence of mutations in the Car9 sequence

Solid-binding peptides that have affinity for inorganic materials are often - but not always capable of inducing their precipitation from precursor species.[5] In addition, several biomolecules capable of precipitating silica have also been found to precipitate titania, and the mechanism of titania biomineralization has been rationalized by comparing it to that of silica formation.[5] Because the Car9 tag has affinity for silica[11,12] and drives the mineralization of titania (Figure 3-5), we made use of the 6 mutants of Table 1 to determine how well-defined changes in the Car9 sequence would affect titania mineralization outcomes.

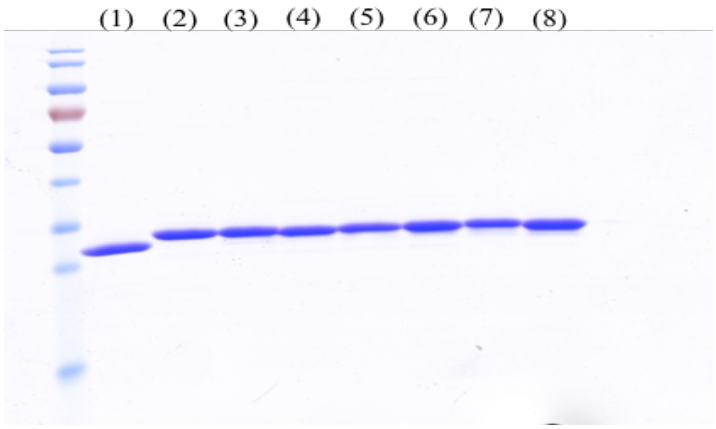

Figure 6. SDS-PAGE of sfGFP-Car9 and its variants. Lanes are: (1) sfGFP; (2) sfGFP-Car9; (3) sfGFP-Car9-F6A; (4) sfGFP-Car9-K8AK11A; (5) sfGFP-Car9-R4QR12Q; (6) sfGFP-Car9-K8HK11H; (7) sfGFP-Car9-P9AG10A; (8) sfGFP-Car9-K7AR12A.

The various fusion proteins were affinity purified on silica and their purity and integrity verified by SDS-PAGE (Figure 6).

CRE-based titania mineralization was performed by depositing 0.5 μL of 25 μM sfGFP-Car9 or of a mutant protein on a 1 % agarose substrate prepared in pH 5.0 citrate buffer and supplemented with 25 mM of TiBALDH (Figure 7 - 8). Previous studies have reported that

synthetic peptides enriched in the basic residues: lysine (K), arginine (R), and histidine (H), are more efficient at inducing titania biomineralization.[2,4,5] In agreement with this observation, replacing positively charged amino acid with neutral residues (R4QR12Q, K7AK11A, K8AR12A mutants), led to a decrease in TiO_2 precipitation efficiency. More surprisingly, the K8HK11H was more efficient than the wild type Car9 at precipitating TiO_2, even though the pI of histidine (7.59) is significantly less than that of lysine (9.74). Even more remarkably, while the P9AG10A and F6A mutations did not change the charge of Car9 domain, titania precipitation efficiency decreased dramatically (Figure 7 and 8). This result suggests that the structure features, such as the presence of a predicted hairpin (P9AG10A mutant) and that of an intact hydrophobic core (F6A mutant), play an important role in TiO_2 mineralization. We note that factors other than positively charged amino acids in titania precipitation by solid binding peptides was also reported by others, such as biomineralization kinetics and peptide local structure. [3-6] To conclude, amino acid substitutions that reduce the number of basic residues in the Car9 sequence decrease sfGFP-Car9 titania mineralization efficiency but local structure appear to play a role that is just as important.

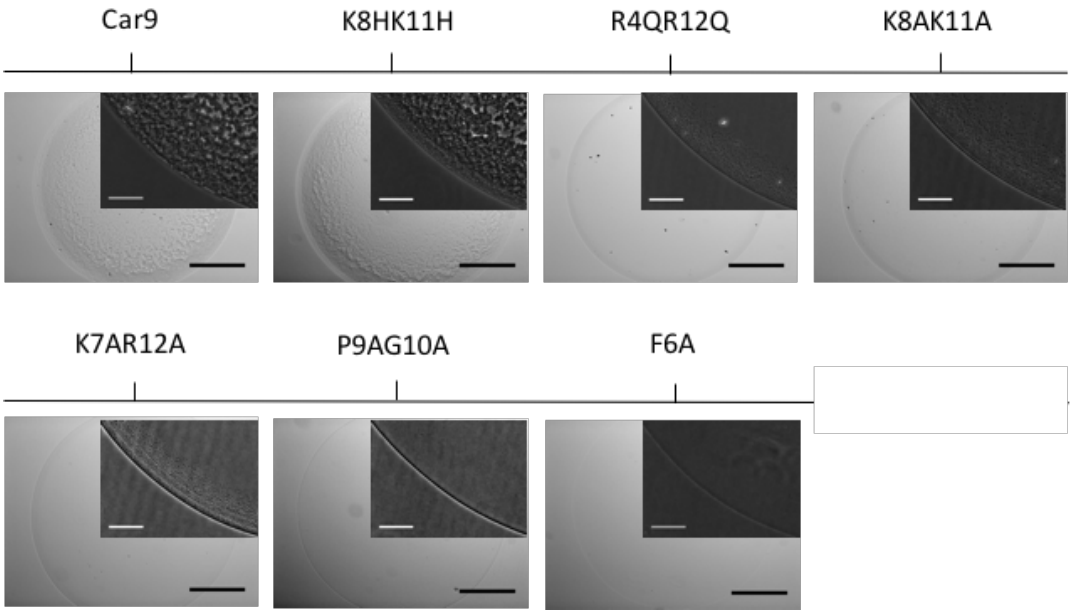

Figure 7. Bright field 4X (large) and 20X (insets) images of titania precipitated by a 0.5 µL droplet of 25 µM sfGFP-Car9 and Car9 mutations. The 1% agarose substrates contained 25 mM TiBALDH and were maintained at pH 5.0 using citrate buffers. Scale bars correspond to 500 µm for 4X images and 100 µm for the insets.

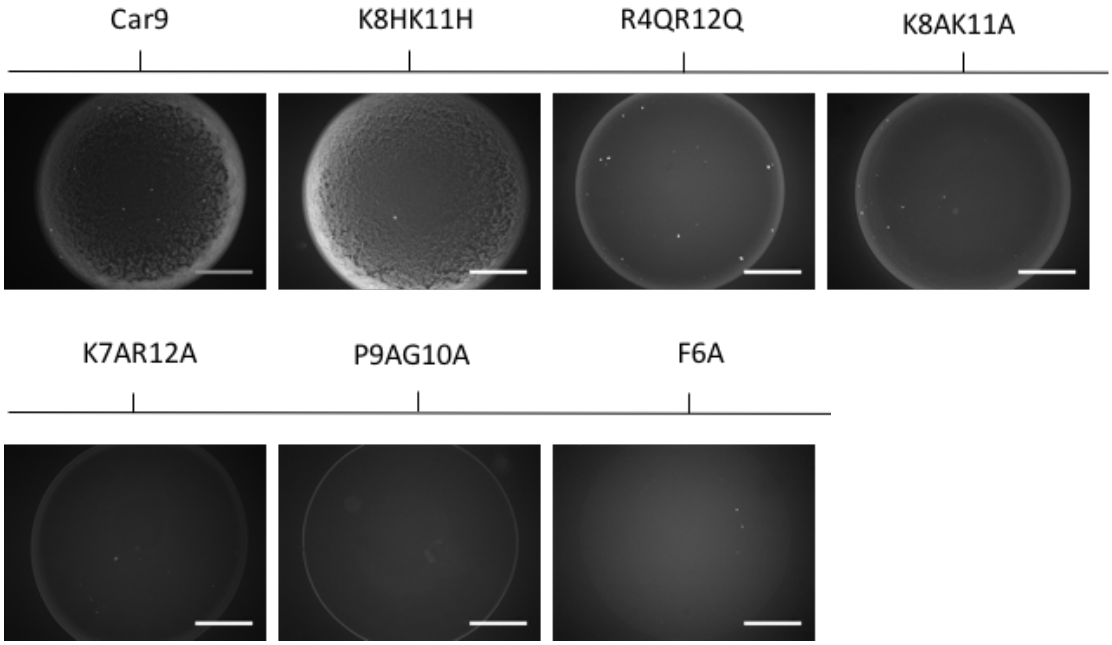

Figure 8. Fluorescent images (4X) of titania precipitated by a 0.5 µL droplet of 25 µM sfGFP-Car9 and Car9 mutations. The 1% agarose substrates contained 25 mM TiBALDH and were maintained at pH 5.0 using citrate buffers. Scale bars correspond to 500 µm.

To gain additional information on the process and quantitatively compare the results, we conducted a fluorescence intensity analysis on fluorescent images as described in Materials and Methods (Figure 9). The area under each curve was integrated to present the amount of titania precipitated by each protein (Table 2).

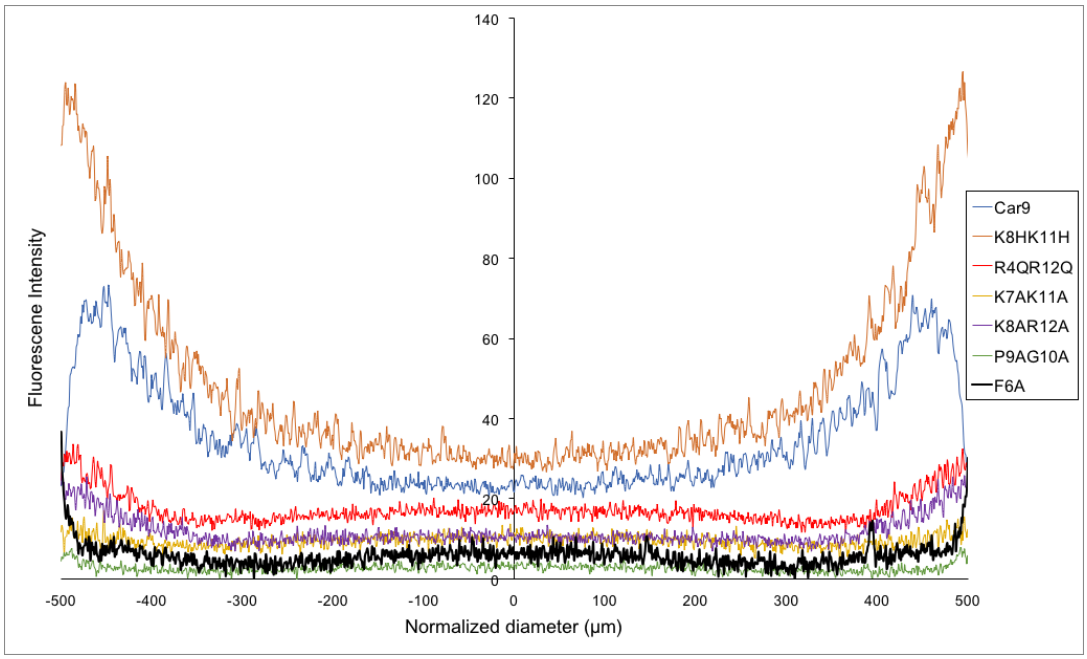

Figure 9. Averaged fluorescence intensity profiles across the diameter of TiO_2 CRE patterns obtained with 25 µM of wild type and mutant sfGFP-Car9 proteins. The diameter of CRE patterns was normalized to 1 mm.

Table 2

Quantification result of Figure 9. Standard deviations were calculated for a minimum of three replicate CRE patterns.

Mutations	Area Under Curve
Car9	35.0±2.7
K8HK11H	49.0±1.3
R4QR12Q	14.3±5.0
K7AR12A	9.8±3.1
K8AK11A	11.3±2.9
P9AG10A	3.0±0.7
F6A	5.9±0.4

Characterization of titania morphology

While the sfGFP-Car9-F6A mutant was ineffective precipitating TiO_2 when used at a concentration of 25 μM (Figure 7), raising its concentration to 50 μM led to a clear TiO_2 pattern, although precipitation efficiency was lower than with sfGFP-Car9 (Figure 10). The material produced by multiple droplets was collected, extensively washed, and imaged by SEM (Figure 11).

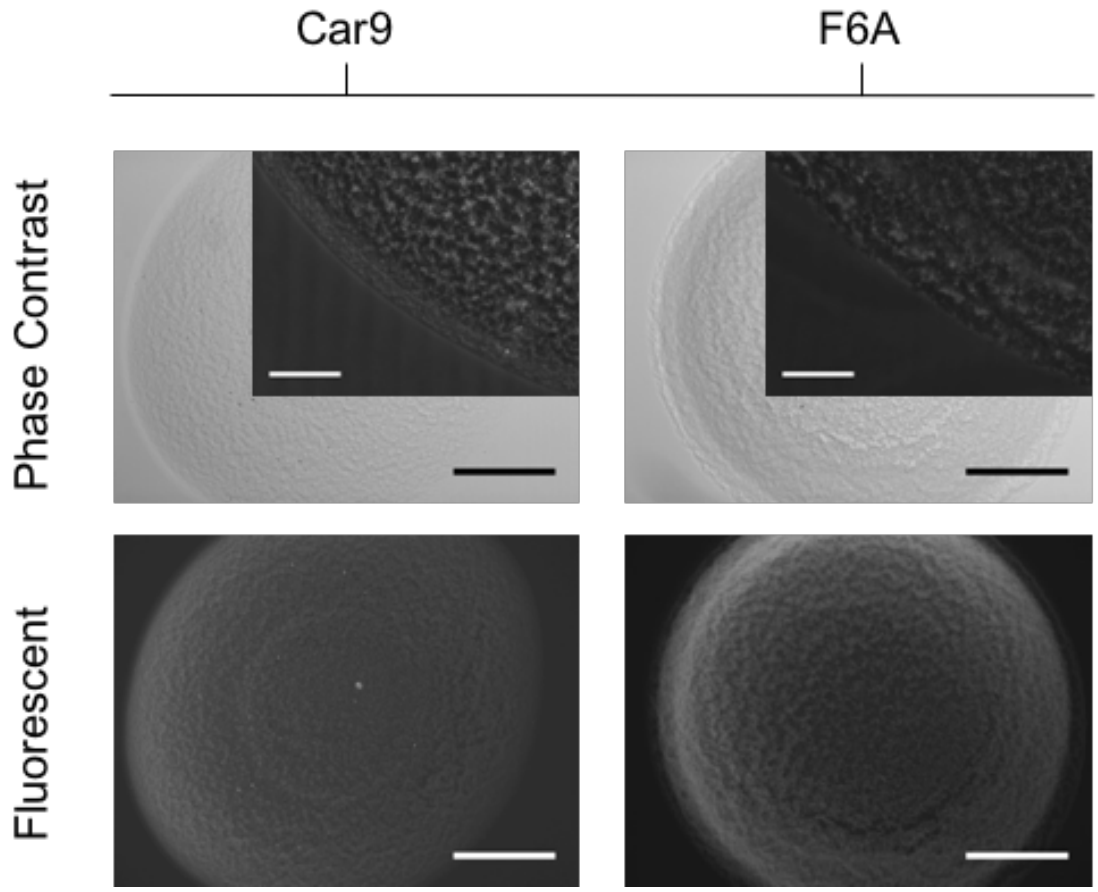

Figure 10. Bright field 4X (large), 20X (inset) and fluorescent 4X images of titania precipitated by a 0.5 μL droplet of 50 μM sfGFP-Car9 and F6A mutants. The 1% agarose substrate contained 25 mM TiBALDH maintained at pH 5.0 using citrate buffer. Scale bars correspond to 500 μm for 4X images and 100 μm for the insets.

Figure 11 e-h show that both samples contained similar particles consisting of spherical nodules ~100-200 nm in diameter interconnected to one another through elongated necks and more extended planar bridges. Thus, at least under these experimental conditions, the F6A mutation seem to affect the rate of TiO_2 precipitation rather than the morphology of the precipitate. We also observed elongated holey structures with characteristic lengths in the 1.5~1.7 μm range in both samples (Figure 11 h). These particles likely correspond to TiO_2 precipitates formed within the inner region of the CRE pattern.

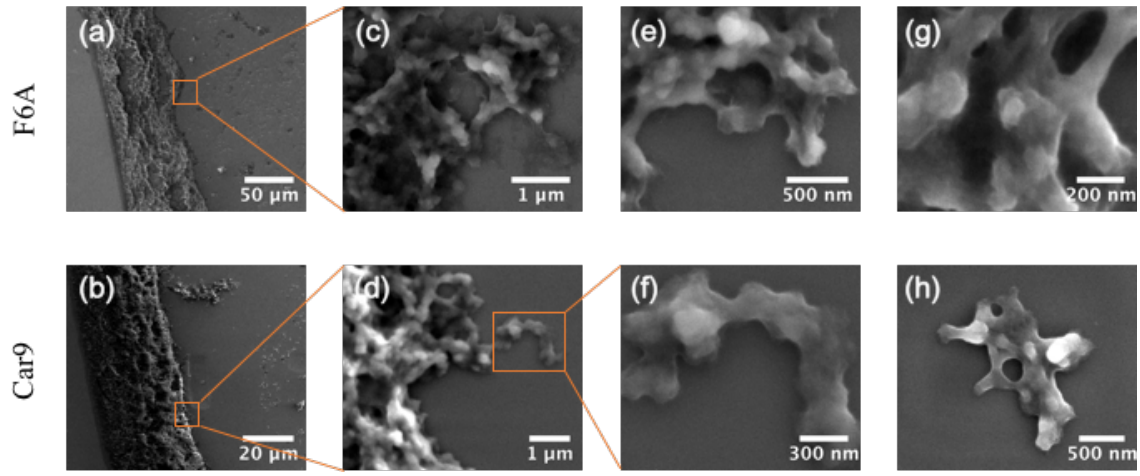

Figure 11. SEM images of titania mineralized by 0.5 μL, 50 μM of sfGFP-Car9 and F6A mutation.

A set of larger particles with slight curvature (Figure 11 a, b) likely correspond to precipitation products formed at the pinned edge of the droplets. Wild type sfGFP-Car9 mineralized narrower (~35 μm) and thicker rope-like structures, compared to the F6A mutant, which yielded wider (~60 μm) and thinner particles. High magnification images of the edges (Figure 11 c, d) revealed that these precipitation products were morphologically similar to the

particles described above except that interconnects were continuous. Thus, while wild type sfGFP-Car9 and its F6A mutant can produce aggregates of different geometries at the pinned edge of the droplet, they appear made up of similar particles. Further investigation will be needed to determine how protein concentration and mutant identity affect these precipitation outcomes and if the crystallography or catalytic properties of the precipitated TiO_2 are altered.

Influence of Car9 locations and number of Car9 tags

To investigate the role of scaffold structural context, we fused the Car9 extension to the N-terminus of sfGFP (producing Car9-sfGFP) and inserted it within a permissive site located within loop 9 of the protein (producing sfGFP::Car9). We also constructed three dual-tags variants (Car9-sfGFP-Car9, sfGFP::Car9-Car9 and Car9-sfGFP::Car9). Proteins were overexpressed in *E. coli.*, purified by silica affinity chromatography, and their purity and structure were verified by with SDS-PAGE (Figure 12). These variants were used in our standard CRE mineralization test to see how Car9 valency and/or position would influence titania mineralization.

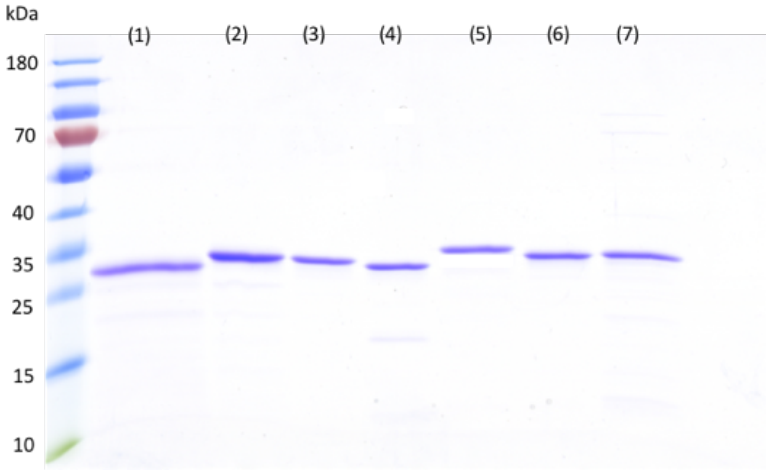

Figure 12. SDS-PAGE of Car9 and Car9 variants: (1) sfGFP (2) sfGFP-Car9 (3) Car9-sfGFP (4) sfGFP::Car9 (5) Car9-sfGFP-Car9 (6) sfGFP::Car9-Car9 (7) Car9-sfGFP::Car9

Result can be seen in Figure 13 (bright field images), Figure 14 (fluorescent images) and Figure 15 (fluorescence intensity analysis).

Placing Car9 at the C-terminus of sfGFP led to an ~ 20% increase in mineralization efficiency relative to fusing it to the protein's N-terminus Car9 (Car9-sfGFP), and a 35% increase compared to placing it in its loop. Increasing the number of Car9 extensions did not significantly increase titania precipitation when Car9-sfGFP-Car9 was compared to sfGFP-Car9, and when Car9-

sfGFP::Car9 was compared to Car9-sfGFP, suggesting that the “strongest” tag location (C-terminal > N-terminal > Loop) dominates the precipitation process. However, combining the “strong” C-terminal tag with the “weak” loop tag on opposite sides of the sfGFP framework to yield sfGFP::Car9-Car9 led to the highest level of titania precipitation. This result suggests that two oppositely located Car9 motifs (e.g., sfGFP::Car9-Car9) are more efficient at inducing titania precipitation than two spatially co-located Car9 motifs (e.g, Car9-sfGFP-Car9). Intriguingly, and as mentioned above, combining two “weak” precipitation motifs (loop and N-terminal tag) opposite to one another did not increase precipitation yields. Yet, it led to a unique precipitation behavior where the edges of the Car9-sfGFP::Car9 droplet did not become pinned at about 1 mm radius like in all other cases, but spreading continued to a radius of 1.5 mm. Characterization of these precipitates will be needed to determine if this distinct precipitation regime leads to unique morphology or crystallography.

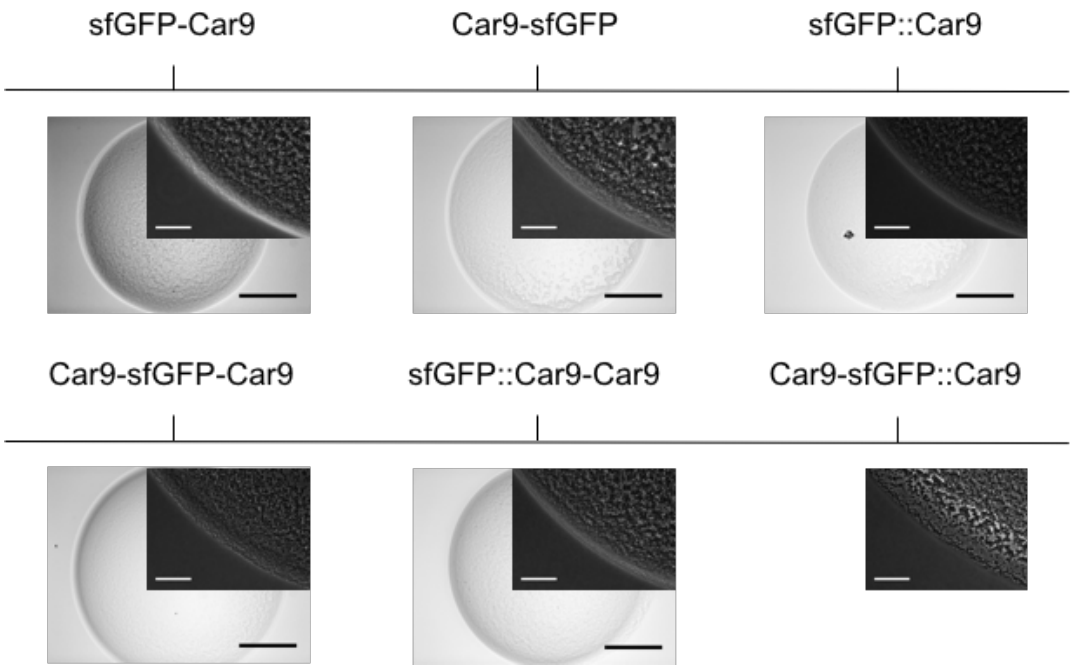

Figure 13. Bright field 4X (large) and 20X (insets) images of titania precipitated by a 0.5 µL droplet of 25 µM sfGFP-Car9 and different Car9 location variants. The 1% agarose substrates contained 25 mM TiBALDH and were maintained at pH 5.0 using citrate buffers. Scale bars correspond to 500 µm for 4X images and 100 µm for the insets.

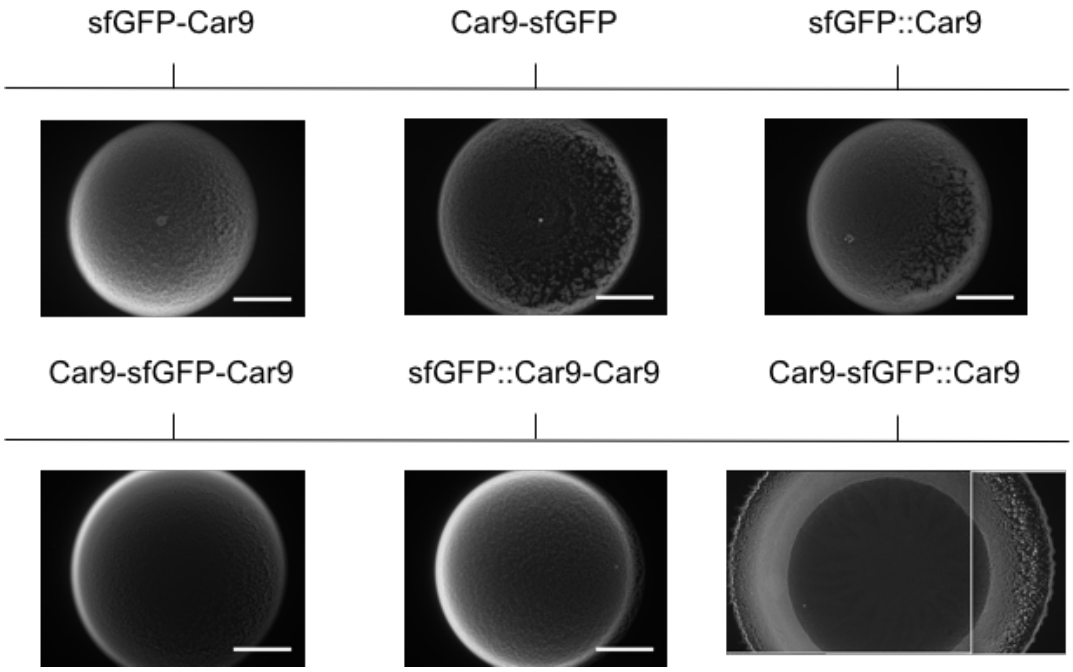

Figure 14. Fluorescent 4X images of titania precipitated by a 0.5 µL droplet of 25 µM sfGFP-Car9 and different Car9 location variants. The 1% agarose substrates contained 25 mM TiBALDH and were maintained at pH 5.0 using citrate buffers. Scale bars correspond to 500 µm.

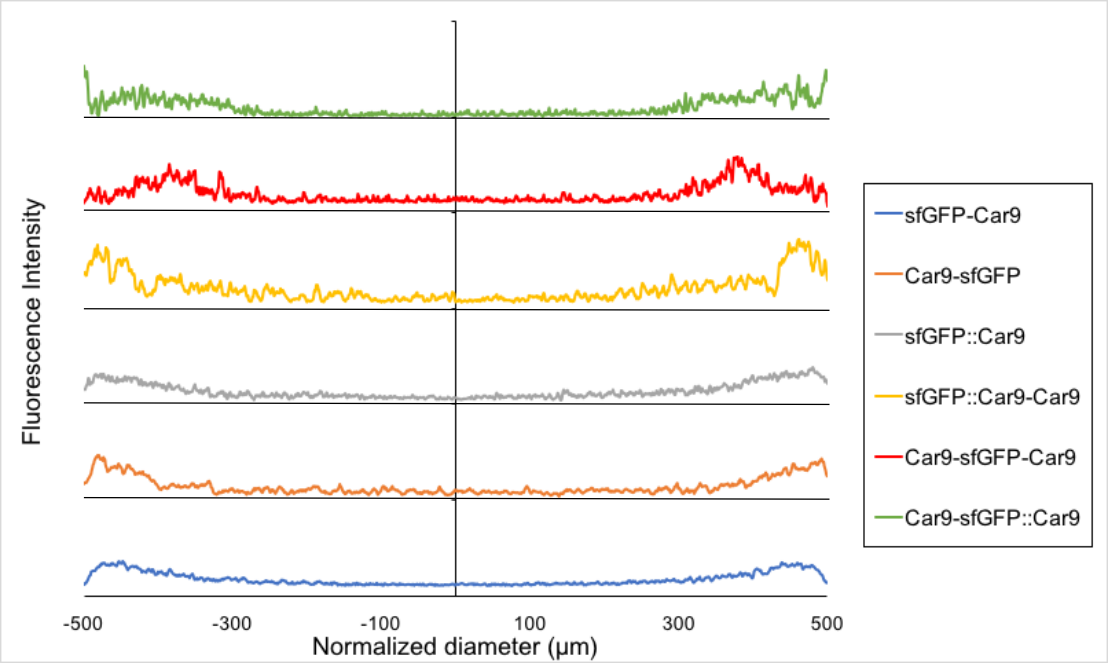

Figure 15. Fluorescence intensity profiles across the diameter of TiO_2 CRE patterns obtained with 25 μM of sfGFP-Car9, Car9-sfGFP, sfGFP::Car9, sfGFP::Car9-Car9, Car9-sfGFP-Car9, Car9-sfGFP::Car9. The diameter of CRE patterns was normalized to 1 mm.

Table 3

Quantification result of Figure 15. Standard deviations were calculated for a minimum of three replicate CRE patterns.

Mutations	Area Under Curve
sfGFP-Car9	35.0±2.7
Car9-sfGFP	29.1±1.6
sfGFP::Car9	25.7±1.8
sfGFP::Car9-Car9	45.8±6.8
Car9-sfGFP-Car9	36.2±6.0
Car9-sfGFP::Car9	29.6±1.6

Influence of the viscosity of protein solution

The diffusion of protein molecules in a liquid is affected by its viscosity. sfGFP-Car9 solutions with viscosities ranging from 0.89 to 1.15 cp (Table 4) were prepared by supplementing protein solutions with different amount of glycerol.[36] CRE mineralization patterns were obtained with our standard approach. As can be seen from the images of Figure 16 and the quantification of the average fluorescence intensity across the diameter of each precipitation pattern (Figure 17), increasing viscosity led to a progressive decrease in the amount of TiO_2 precipitating at the pinned edge and a decrease in the granularity of the deposit.

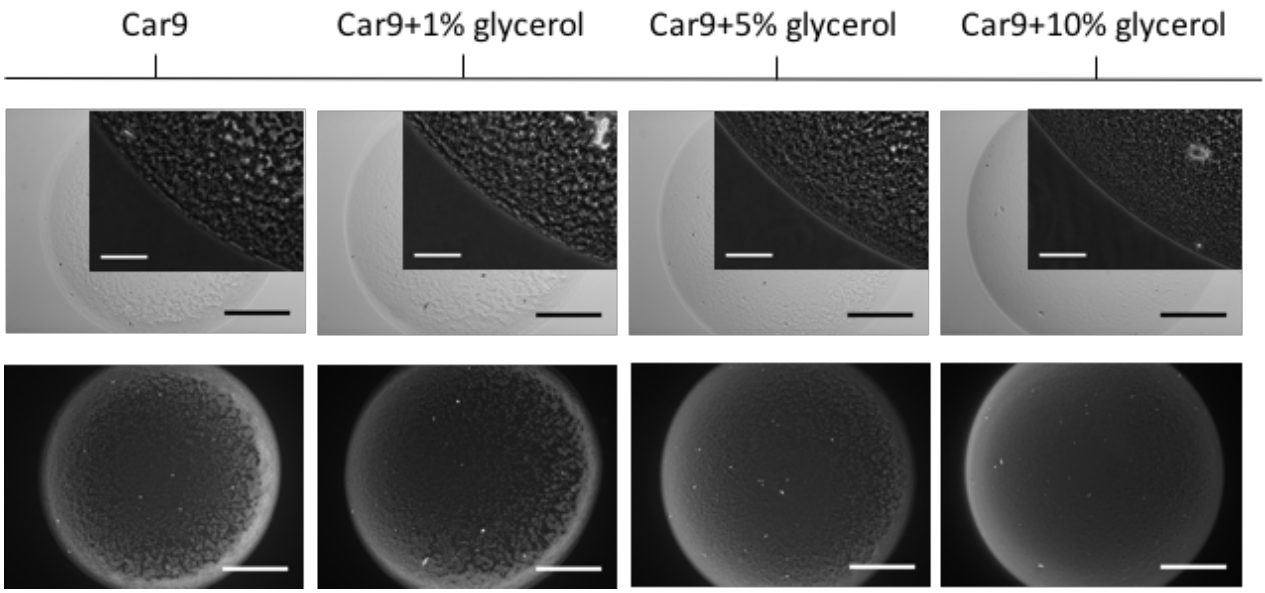

Figure 16. Effect of the solution viscosity on the production of CRE patterns by 25 µM sfGFP-Car9 supplemented with the indicated concentration of glycerol in 20 mM Tris-HCl buffers. Image from top to bottom: Bright field (4X), bright field inset (20X) and fluorescence (4X) focused at edge of the deposit patterns. Scale bars correspond to 500 µm for 4X images and 100 µm for the insets.

In the presence of 10% (v/v) glycerol, which corresponds to a viscosity of 1.15 cp, we observed a smooth precipitate and fairly even distribution of the material across the diameter of the CRE pattern (Figure 17). We attribute this result to increased resistance to radially outward flow and a concomitant decrease in protein mobility which leads to more uniform mineralization.[22]

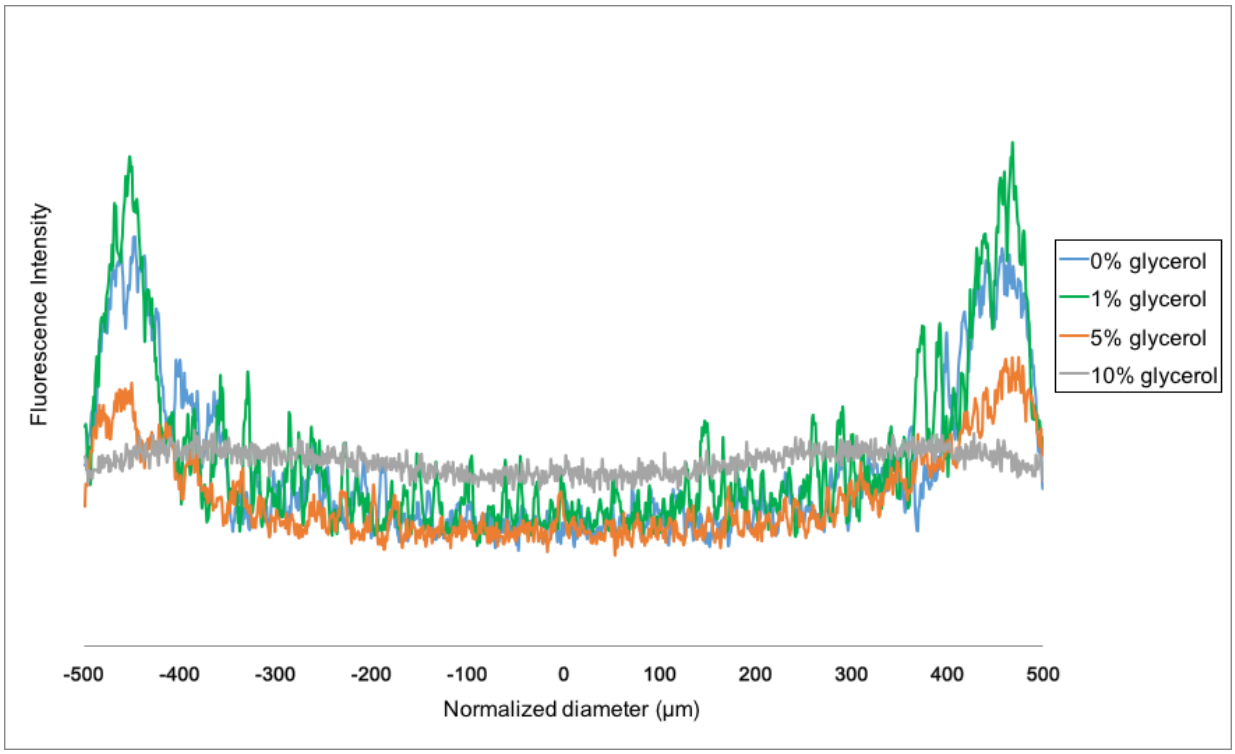

Figure 17. Fluorescence intensity profiles across the diameter of TiO_2 CRE patterns obtained with 25 μM of sfGFP-Car9 in pH 5.0 citrate buffer supplemented with no glycerol (blue), 1% (green), 5% (orange) and 10% glycerol (gray).

Table 4

Quantification result of Figure 17

	Viscosity (cp)	Diffusion Coefficient (cm^2/s)	Area under curve
0% Glycerol	0.89	$1.10*10^{-6}$	41.0
1% Glycerol	0.91	$1.08*10^{-6}$	44.0
5% Glycerol	1.00	$0.98*10^{-6}$	34.0
10% Glycerol	1.15	$0.85*10^{-6}$	42.0

Influence of protein framework

To detemine if the Car9 extension would improve titania biomineralization when fused to protein scaffolds other than sfGFP, we used two additional C-terminal Car9 fusion to mCherry and maltose-binding protein (MBP).[11] Proteins (0.5 µL of 25 µM solutions) were deposited on a 1% agarose substrate prepared in citrate buffer and supplemented with 25 mM TiBALDH, as in previous experiments. Figure 18 shows that while mCherry-Car9 was as efficient or better than sfGFP-Car9 at inducing titania precipitation, MBP-Car9 was unable to do so under the same conditions. This result is surprising in light of the fact that MBP-Car9 binds to silica and may reflect a need for pH optimization.

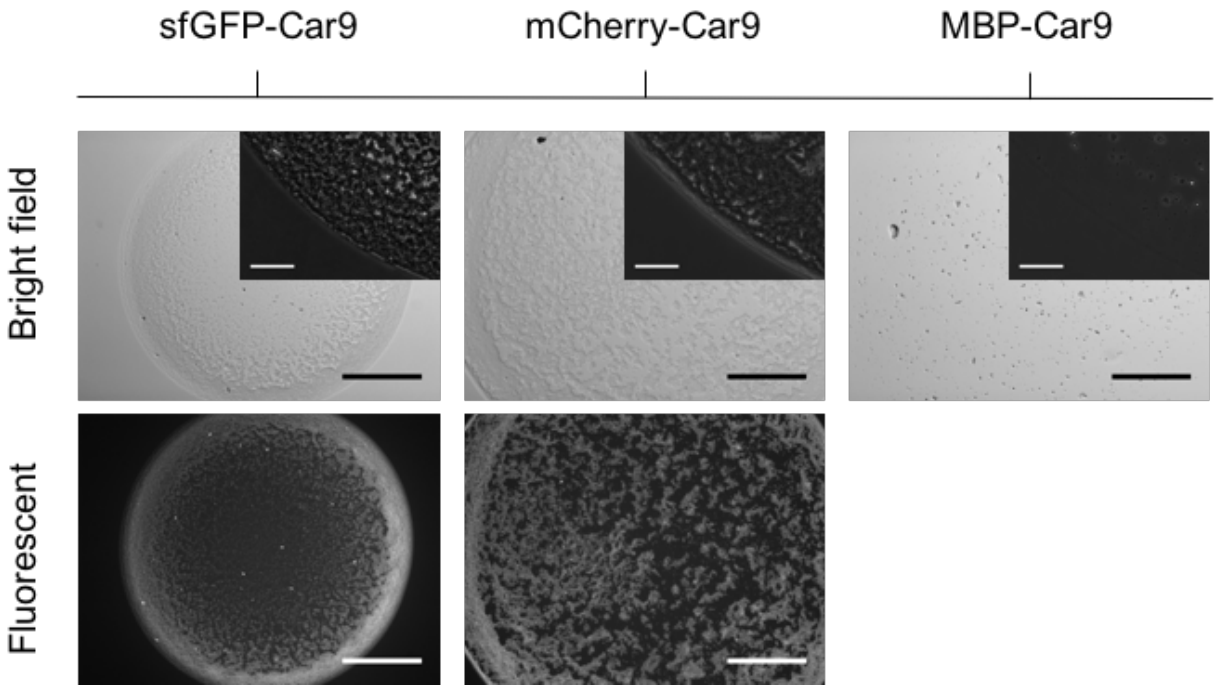

Figure 18. Bright field images 4X (large), 20X (insets) and fluorescent images 4X of titania precipitated by a 0.5 µL droplet of 25 µM sfGFP-Car9, mCherry-Car9 and MBP-Car9. The 1% agarose substrates contained 25 mM TiBALDH and were maintained at pH 5.0 using citrate buffers. Scale bars correspond to 500 µm for 4X images and 100 µm for the insets.

Conclusions

We have taken advantage of the coffee ring effect (CRE) to study how derivatives of sfGFP incorporating one or more Car9 silica-binding peptides modulate titania precipitation under non-equilibrium conditions. In the CRE-based biomineralization approach developed herein, a protein solution droplet is deposited on a thin agarose hydrogel supplemented with the titanium precursor TiBALDH. As evaporation-induced outwards flow transports the protein towards the pinned triple line, TiO_2 precipitation patterns that consume the protein are observed.

We have found that fusing a Car9 extension to the sfGFP framework allows for titania precipitation to occur under less acidic conditions (pH 5.0 compared to pH 4.8 for wild type sfGFP alone), and that mutating Car9 basic and structural residues decrease titania precipitation efficiency. We have also found that placement of the Car9 tag within the sfGFP scaffold (C-terminal fusion, N-terminal fusion, or permissive loop insertion) has subtle effects on the extent titania precipitation, and that multivalent constructs can influence both the amount of TiO_2 precipitated and the mineralization pattern. Taken together, our results indicate that the structural context in which positively charged amino acids are presented to the solvent, and the chemistry and structure of Car9 attachment points are important factors

in controlling the fine balance between protein transport, titania binding, and titania precipitation.

Because our SEM studies indicate that titania precipitated in the interior region of the droplet and the pinned edge differ in interconnectivity, future work should focus on how the above parameters can be tuned to access unique morphologies, and possibly crystallographies.

Reference

[1] Sewell, Sarah L., Ryan D. Rutledge, and David W. Wright. "Versatile biomimetic dendrimer templates used in the formation of TiO 2 and GeO 2." *Dalton Transactions* 29 (2008): 3857-3865.

[2] Ahn, Sungjun, Sangwoo Park, and Sang-Yup Lee. "Oligo (L-lysine)-induced titanium dioxide: Effects of consecutive lysine on precipitation." *Journal of Crystal Growth* 335.1 (2011): 100-105.

[3] Dickerson, Matthew B., et al. "Identification and design of peptides for the rapid, high-yield formation of nanoparticulate TiO2 from aqueous solutions at room temperature." *Chemistry of Materials* 20.4 (2008): 1578-1584.

[4] Hernández-Gordillo, Armin, et al. "Biomimetic Sol–Gel Synthesis of TiO2 and SiO2 Nanostructures." *Langmuir* 30.14 (2014): 4084-4093.

[5] Puddu, Valeria, et al. "Titania binding peptides as templates in the biomimetic synthesis of stable titania nanosols: Insight into the role of buffers in peptide-mediated mineralization." *Langmuir* 29.30 (2013): 9464-9472.

[6] Choi, Noori, et al. "The interplay of peptide sequence and local structure in TiO 2 biomineralization." *Journal of inorganic biochemistry* 115 (2012): 20-27.

[7] Coyle, Brandon L., Weibin Zhou, and François Baneyx. *Protein-aided mineralization of inorganic nanostructures*. Caister Academic Press: Norwich, UK, 2013.

[8] Cole, Kathryn E., et al. "Peptide-and long-chain polyamine-induced synthesis of micro-and nanostructured titanium phosphate and protein encapsulation." *Chemistry of materials* 18.19 (2006): 4592-4599.

[9] West, R.H., Celnik, M.S., Inderwilidi, O.R., Kraft, M., Beran, J.O. & Green, W.H. Toward a comprehensive model of the synthesis of TiO_2 particles from $TiCl_4$. *Ind. Eng. Chem. Res.* 46, 6147-6156 (2007)

[10] Chiu, David, et al. "Biomineralization and size control of stable calcium phosphate core–protein shell nanoparticles: potential for vaccine applications." *Bioconjugate chemistry* 23.3 (2012): 610-617.

[11] Coyle, Brandon L., and François Baneyx. "A cleavable silica-binding affinity tag for rapid and inexpensive protein purification." *Biotechnology and bioengineering* 111.10 (2014): 2019-2026.

[12] Coyle, Brandon L., Marco Rolandi, and François Baneyx. "Carbon-binding designer proteins that discriminate between sp2-and sp3-hybridized carbon surfaces." *Langmuir* 29.15 (2013): 4839-4846.

[13] Care, Andrew, Peter L. Bergquist, and Anwar Sunna. "Solid-binding peptides: smart tools for nanobiotechnology." *Trends in biotechnology* 33.5 (2015): 259-268.

[14] Baneyx, François, and Daniel T. Schwartz. "Selection and analysis of solid-binding peptides." *Current opinion in biotechnology* 18.4 (2007): 312-317.

[15] Deegan, Robert D., et al. "Capillary flow as the cause of ring stains from dried liquid drops." *Nature* 389.6653 (1997): 827-829.

[16] Deegan, Robert D., et al. "Contact line deposits in an evaporating drop." *Physical review E* 62.1 (2000): 756.

[17] Deegan, Robert D. "Pattern formation in drying drops." *Physical review E* 61.1 (2000): 475.

[18] Devineau, Stéphanie, et al. "Protein adsorption and reorganization on nanoparticles probed by the coffee-ring effect: application to single point mutation detection." *Journal of the American Chemical Society* 138.36 (2016): 11623-11632.

[19] Kajiya*, Tadashi, Daisaku Kaneko, and Masao Doi. "Dynamical visualization of “coffee stain phenomenon” in droplets of polymer solution via fluorescent microscopy." *Langmuir* 24.21 (2008): 12369-12374.

[20] Bhardwaj, Rajneesh, et al. "Self-assembly of colloidal particles from evaporating droplets: role of DLVO interactions and proposition of a phase diagram." *Langmuir* 26.11 (2010): 7833-7842.

[21] Nguyen, Tuan AH, Marc A. Hampton, and Anh V. Nguyen. "Evaporation of nanoparticle droplets on smooth hydrophobic surfaces: the inner coffee ring deposits." *The Journal of Physical Chemistry C* 117.9 (2013): 4707-4716.

[22] Cui, Liying, et al. "Suppression of the coffee ring effect by hydrosoluble polymer additives." *ACS applied materials & interfaces* 4.5 (2012): 2775-2780.

[23] Berteloot, Guillaume, et al. "Evaporation of a sessile droplet: Inside the coffee stain." *Journal of colloid and interface science* 370.1 (2012): 155-161.

[24] Still, Tim, Peter J. Yunker, and Arjun G. Yodh. "Surfactant-induced Marangoni eddies alter the coffee-rings of evaporating colloidal drops." *Langmuir* 28.11 (2012): 4984-4988.

[25] Crivoi, Alexandru, and Fei Duan. "Three-dimensional Monte Carlo model of the coffee-ring effect in evaporating colloidal droplets." *Scientific reports* 4 (2014).

[26] Keller, Joseph B., and Sol I. Rubinow. "Recurrent precipitation and Liesegang rings." *The Journal of Chemical Physics* 74.9 (1981): 5000-5007.

[27] Krug, Hans-Jürgen, and Hermann Brandtstädter. "Morphological characteristics of Liesegang rings and their simulations." *The Journal of Physical Chemistry A* 103.39 (1999): 7811-7820.

[28] Swift, Brian J., et al. "Streamlined synthesis and assembly of a hybrid sensing architecture with solid binding proteins and click chemistry." *Journal of the American Chemical Society* 139.11 (2017): 3958.

[29] Ruzin, 1999 Plant Microtechnique and Microscopy

[30] Schirmer, N. C.; Strö hle, S.; Tiwari, M. K.; Poulikakos, D. Adv. Funct. Mater. 2011, 21, 388−395.

[31] Park, Jungho, and Jooho Moon. "Control of colloidal particle deposit patterns within picoliter droplets ejected by ink-jet printing." *langmuir* 22.8 (2006): 3506-3513.

[32] Deng, Yang, et al. "Transport at the air/water interface is the reason for rings in protein microarrays." *Journal of the American Chemical Society* 128.9 (2006): 2768-2769.

[33] Wong, Tak-Sing, et al. "Nanochromatography driven by the coffee ring effect." *Analytical chemistry* 83.6 (2011): 1871-1873.

[34] Sewell, Sarah L., and David W. Wright. "Biomimetic Synthesis of Titanium Dioxide Utilizing the R5 Peptide Derived from Cylindrotheca fusiformis." *Chemistryof materials* 18.13 (2006): 3108-3113.

[35] Deng, Yuan-Fu, et al. "Speciation of water-soluble titanium citrate: Synthesis, structural, spectroscopic properties and biological relevance." *Polyhedron* 26.8 (2007): 1561-1569.

[36] Gregory, Sonia, and Henryk Mach. "Adaptation of a High-Pressure Liquid Chromatography System for the Measurement of Viscosity." *Chromatography* 1.2 (2014): 55-64.

Supplementary Data

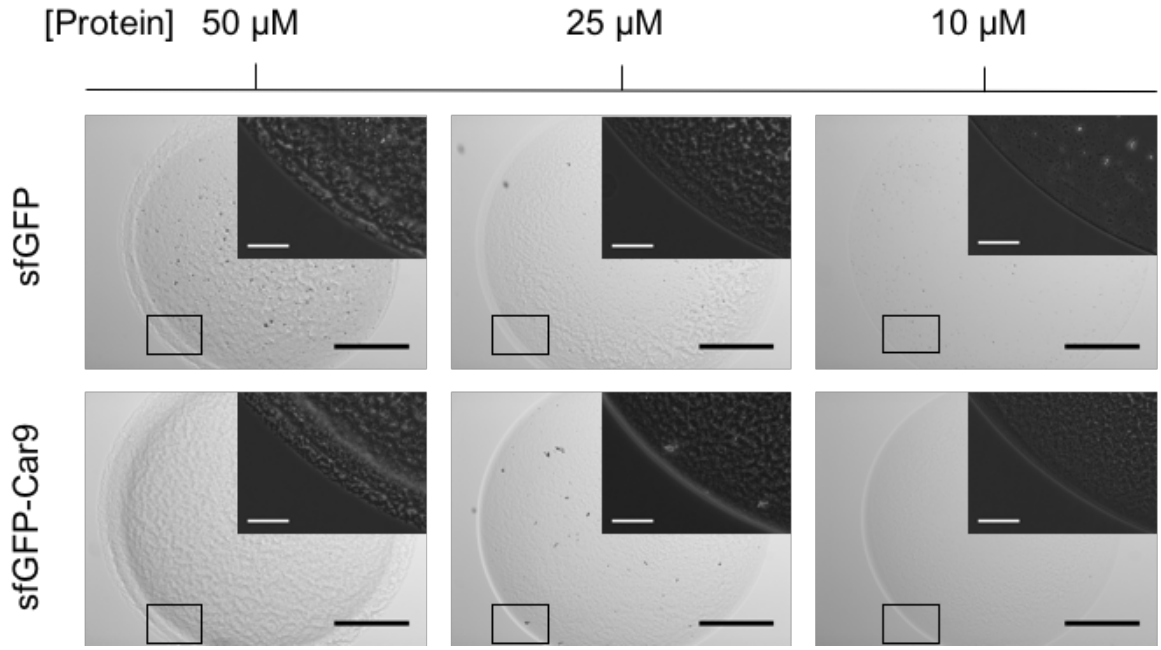

Figure S1(A). Bright field images 4X (large) and 20X (insets) of titania precipitated by a 0.5 µL droplet of sfGFP or sfGFP-Car9 at the indicated concentrations. The 1% agarose substrates contained 25 mM TiBALDH and were maintained at pH 4.8 using citrate buffers. Scale bars are 500 µm (large) and 100 µm (insets).

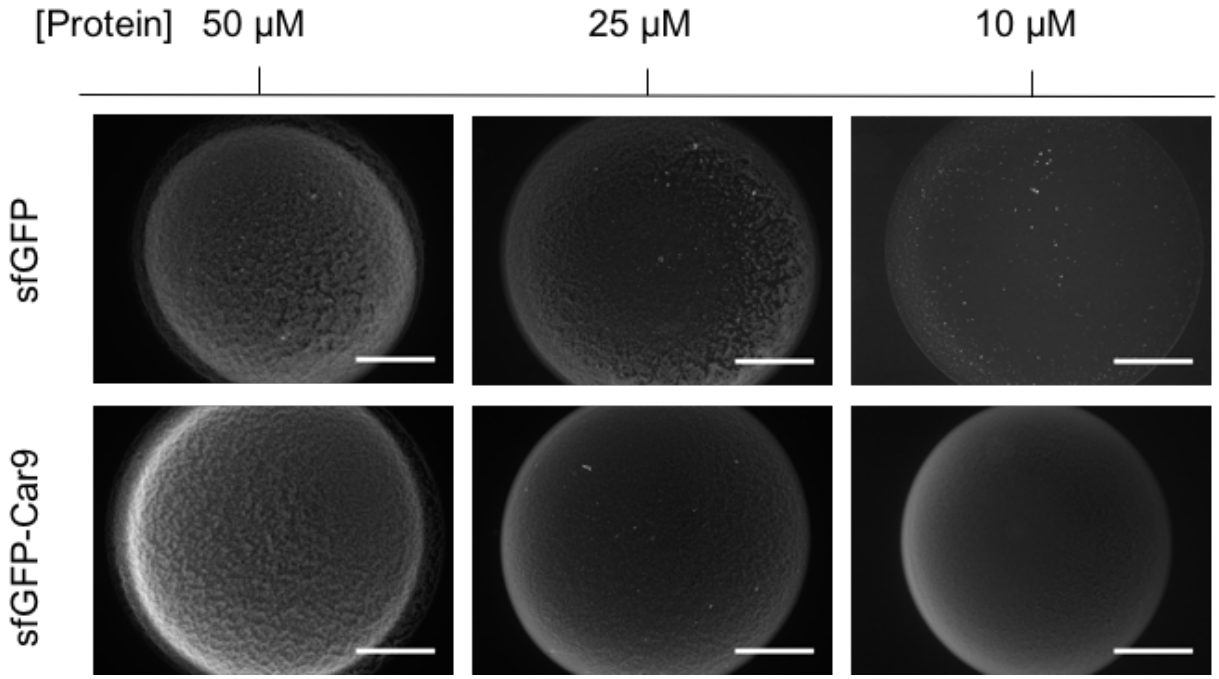

Figure S1(B). Fluorescent images 4X of titania precipitated by a 0.5 µL droplet of sfGFP or sfGFP-Car9 at the indicated concentrations. The 1% agarose substrates contained 25 mM TiBALDH and were maintained at pH 4.8 using citrate buffers. Scale bars are 500 µm.

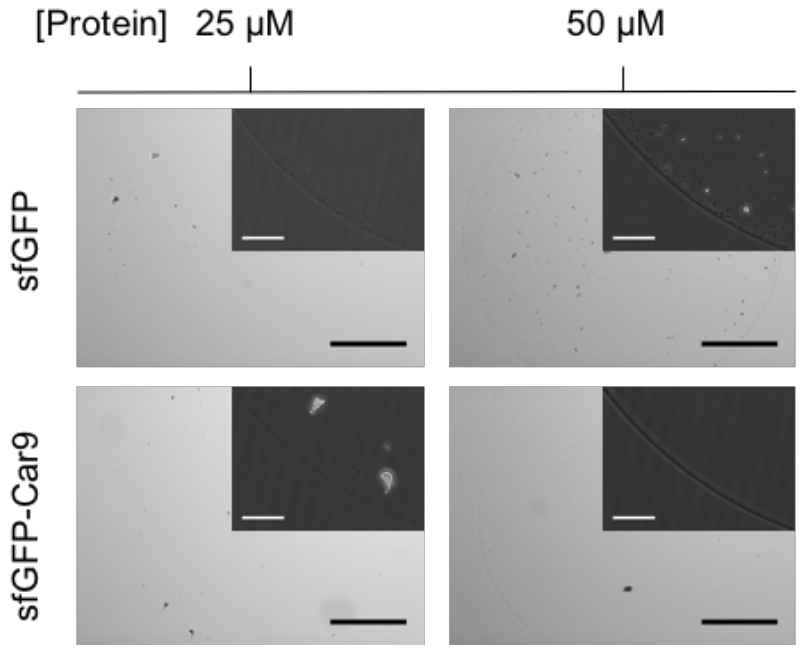

Figure S2(A). Bright field images 4X (large) and 20X (insets) of titania precipitated by a 0.5 μL droplet of sfGFP or sfGFP-Car9 at the indicated concentrations. The 1% agarose substrates contained 25 mM TiBALDH and were maintained at pH 5.2 using citrate buffers. Scale bars are 500 μm (large) and 100 μm (insets).

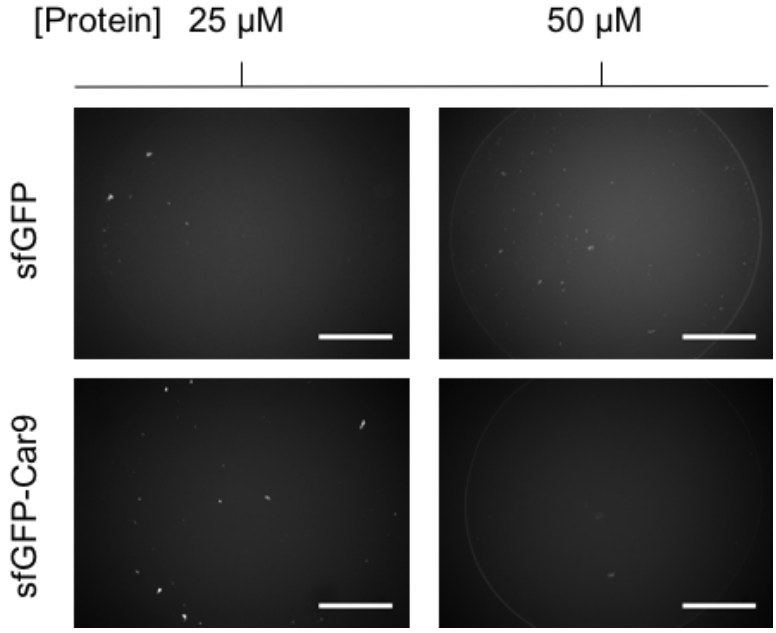

Figure S2(B). Fluorescent images 4X of titania precipitated by a 0.5 μL droplet of sfGFP or sfGFP-Car9 at the indicated concentrations. The 1% agarose substrates contained 25 mM TiBALDH and were maintained at pH 5.2 using citrate buffers. Scale bars are 500 μm.

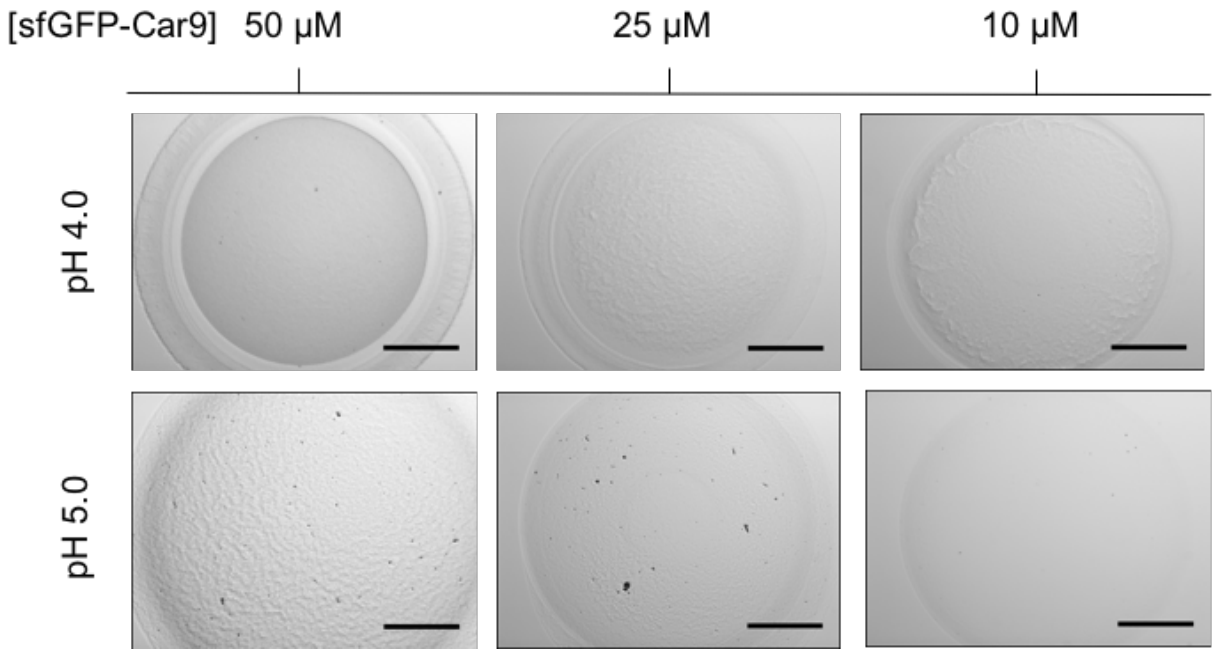

Figure S3(A). Bright field images 4X of titania precipitated by a 0.5 µL droplet of sfGFP-Car9 at the indicated concentrations. The 1% agarose substrates contained 25 mM TiBALDH and were maintained at pH 4.0 or 5.0 using citrate buffers. Scale bars are 500 µm.

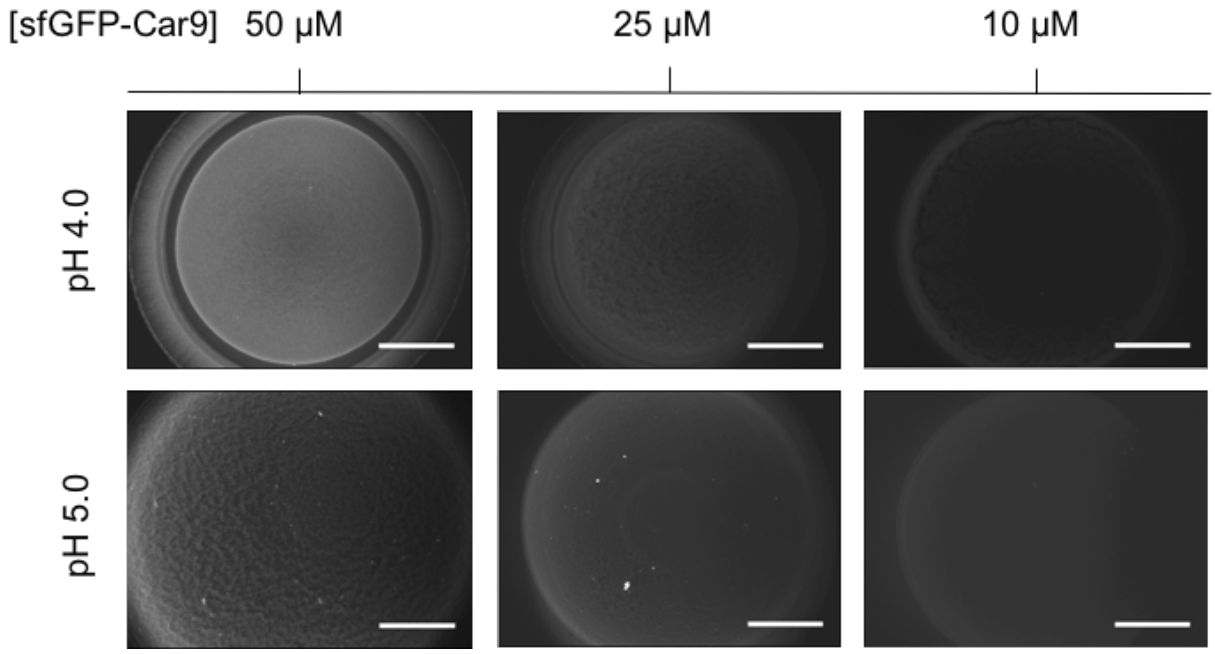

Figure S3(B). Fluorescent images 4X of titania precipitated by a 0.5 µL droplet of sfGFP-Car9 at the indicated concentrations. The 1% agarose substrates contained 25 mM TiBALDH and were maintained at pH 4.0 or 5.0 using citrate buffers. Scale bars are 500 µm.